

# Semi-Micro Bounding Surface Model for Anisotropic Sand

**Seyed Amirodin Sadrnejad**

*Prof., Dept. of Civil Eng, K.N. Toosi University of Tech., Tehran, Iran  
e-mail: sadrnejad@kntu.ac.ir*

## ABSTRACT

This paper deals with the development of a numerical model providing reliable estimates of the loading of a sand box with buried steel pipe subjected to cyclic loading. The reliability test is based on two physically and statistically independent sets of experiments.

The first set is related to elastoplastic material modeling and the second set to structural model verification. Since model verification can be accomplished successfully, the developed model is well suited to provide prognoses of the loading of a sand-buried steel pipe for dynamic loading scenarios.

Accordingly, an induced anisotropic plasticity model predicting dynamic behaviour of sand is presented. The model incorporates the critical/steady state concept that postulates the existence of a state where sand continuously deforms at a certain constant effective stress depending two main parameters of both initial bulk parameters (i.e. void ratio or relative density) and stress level (i.e. mean stress). The local instability of saturated sand within post-liquefaction is highly dependent on the residual inherent/induced anisotropy, bedding plane effects, and stress/strain path.

Most of the models developed using stress/strain invariants are not capable of identifying the parameters depending on orientation such as fabric. This is mainly because stress/strain invariants are quantities similar to scalar quantities and not capable of carrying directional information with themselves.

The constitutive equations of the model are derived within the context of non-linear elastic behaviour of the whole medium and plastic sliding of interfaces of predefined multi-planes.

The proposed multi-plane based model is capable of predicting the behaviour of soils on the basis of plastic sliding mechanisms, elastic behaviour of particles and possibilities to see the micro-fabric effects as natural anisotropy as well as induced anisotropy in plasticity.

The comparison of model results with experiments under both drained and undrained tests show the capability and power model in predicting of soil behaviour under any condition in soil structures.

**KEYWORDS:** Multi-plane, Elastic-plastic, Model, Bounding surface, anisotropic sand

## INTRODUCTION

A steel pipe buried in sand is considered in this study. If a dynamic cyclic loading is applied onto the overburden of the pipe, the kinetic energy of the loading is transformed into other types of energy. Most of this energy is transformed such that inelastic deformations of the overburden are produced. Other parts of the input energy are transmitted through the sand via elastoplastic waves to the buried pipe, which represents a rather stiff component of the statically over determined load-carrying system. Accordingly, the sand acts as an energy-absorbing and load-distributing system.

This contribution deals with the development of an analysis tool that permits reliable predictions of the loading of sand buried steel pipeline subjected to cyclic loading.

Concern the material behavior, multi-plane theory (framework) is semi-micromechanical tool based on obtaining the numerical relation (integration) between inter granular behaviors (microscopic behavior), and mechanical properties (macroscopic behavior) in the form of (upon any non-linear) a constitutive law. In other words, in this framework material properties stem from properties of each component; therefore, achievement to stress-strain behavior of soils is possible by surveying inter granular (mechanical behavior) displacements.

Multi-plane framework cannot predict the behavior of material independently, and it must be declared in the form of a constitutive law. This constitutive law obtains the treatment of each plane; by using this framework the overall behavior is, therefore, acquired by accumulating behaviors of all defined planes. In this way there are no limitations to choose the constitutive law. The constitutive model employed in this paper is Unified 3D Critical State Bounding-Surface model for Soils Incorporating Continuous Plastic Loading under Cyclic Paths proposed by Crouch et al. [1] and some points in general about this model:

Capability of all constitutive models, which are used to evaluate the mechanical behavior of the soils, is a result of the ability of non-linear computational analysis to furnish realistic simulations of the soil's treatment. Therefore, the Endeavour to achieve a model with uncomplicated constitutive law and reliable outcome goes on. Despite the fact that numerous formulations have been presented over the past 50 years, there have not been enough eligible models to predict different types of soils' behavior under both cohesive/noncohesive and also drained/undrained conditions accurately. The utility of this model is not only simple organization in the form of classical plasticity, but also it can manipulate all sorts of soils including clay, sand and silt. It can, moreover, pursue, and describe the plasticity of the soils in the variety of surfaces, and using this feature provides us to allocate different properties in each surface.

Even though clays and sands have unlike microstructures, their macroscopic manners (ignoring viscous and thermal effects) demonstrate lots of common features like:

- 1- Dependency of strains on the effective stresses instead of the total stresses.
- 2- Under shearing circumstances, hardening connects to non-linear compaction, whereas softening associated with non-linear dilation.
- 3- Plastic compaction occurs below the critical state line (low stress ratios), in contrast plastic dilation takes place above the critical state line (high stress ratios).
- 4- Failure happens in the critical state when there is no change in stress state or volume.
- 5- Shear strength depends on mean effective stress.
- 6- For the normally consolidated clays and loose sands, the drained strengths are higher than undrained strengths; on the other hand, for the heavily consolidated clays and dense sands, the drained strengths are lower than undrained strengths, in the same initial void ratio and confining pressure
- 7- Rotation of principal stress/strain axes and lack of coaxialities
- 8- Induced/inherent anisotropy and the changes of fabric behavior
- 9- Moisture effects on mechanical behavior, etc.....

For the first time presented constitutive formulation in this paper, which shows a volumetric plastic hardening relation based on the bounding surface plasticity model, introduced by Dafalias and Herrmann[2] for isotropic clays.

The main features of presented model are:

Combined use of radial and deviatoric mapping rules to define the loading surface, and the use of an apparent normal consolidation line for sands. During hydrostatic loading, the volumetric plastic strains are captured by means of the radial mapping rule. Usually clays and especially normally over

consolidated ones lie on the bounding surface, or in the radial mapping region. However, sands usually are located in the deviatoric mapping region. As a result, clays and sands are operating in two different zones of similarly shaped bounding surfaces.

Use of a non-associated flow rule where the ratio of the rates of volumetric plastic strain to deviatoric plastic strain (plastic dilatancy rate) is a function only of the ratio of deviatoric to mean effective stresses.

- Adoptions of a bi-linear critical state line the plane of the void ratio versus logarithm of mean effective stress. This feature was introduced by Been et al to support a reduced slope of the critical state line in the high void ratio range for sands [3].
- Inclusion of a sub-elliptic, or super-elliptic, segment in the plastic dilatancy surface for stress ratios less than critical.
- Use of elliptic segments [4] in the deviatoric plane.
- Incorporation of a plastic stiffening effect for cyclic paths which repeatedly load in the same deviatoric direction by means of memorizing the maximum previous stress excursion.
- Definition of 26 surfaces for whole sphere (13 independent planes for one semi-sphere are identical to another semi-sphere's planes) to transfer plasticity on them. These planes provide an anisotropic behavior to model; also, they introduce different plasticity on each surface which is active during the given stress paths [5, 6].

Details of each feature are completely described in three-dimensional space. After introducing the effective stress and strain vectors and the normal and shear stresses on each plane, the governing equations for bounding-surface plasticity are implemented. The following are subsequently defined: first, definition of planes and their local axes; second, the bounding surface for each plane; next, the dependence of the critical state line on the void ratio together with the (apparent) normal consolidation line and rebound line for each plane; then, the loading surface for each plane; moreover the plastic strain rate direction, and finally, the bounding and additive plastic moduli for each plane. It is demonstrated that the proposed model can culminate in precise and accurate results over a wide range of void ratios and confinement pressures for soils.

In the (At) failure condition, failing of all planes is not compulsory. Fracture in each plane relates to the stress/strain levels on this plane, and this feature may be used to estimate the fracture direction of an element (at a point), and as a result, the probable fracture directions of a soil structure can be obtained. However, the on-plane strain conditions reveal the type of fracture discontinuity (compressive, sheared, or tensile,...).

## CONSTITUTIVE EQUATION OF MULTI-PLANE BOUNDING SURFACE MODEL

The constitutive equations of multi-plane model starts with the classical decomposition of strain and strain increments under the concept of elastic-plasticity in elastic and plastic parts are schematically written as follows:

$$\boldsymbol{\varepsilon} = \boldsymbol{\varepsilon}^e + \boldsymbol{\varepsilon}^p \quad (1)$$

$$d\boldsymbol{\varepsilon} = d\boldsymbol{\varepsilon}^e + d\boldsymbol{\varepsilon}^p \quad (2)$$

The increment of elastic strain ( $d\boldsymbol{\varepsilon}^e$ ) is related to the increments of effective stress ( $d\boldsymbol{\sigma}$ ) by:

$$d\boldsymbol{\varepsilon}^e = [D^e]^{-1} d\boldsymbol{\sigma} \quad (3)$$

$[D^e]^{-1}$  is elastic compliance matrix, usually assumed as linear and is obtained as follows:

$$D_{ijkl}^e = (K - \frac{2}{3}G)\delta_{ij}\delta_{kl} + G(\delta_{ik}\delta_{jl} + \delta_{il}\delta_{jk}) \quad (4)$$

$K$  and  $G$  are bulk and the shear modulus, respectively. Any kind of non-linearity as the change of these parameters may be applied in an incremental algorithm. A simple form of this change in shear modulus is as follows:

$$G/G_0 = P_a[(2.97 - e)^2 / (1 + e)][P/P_a]^h \quad (5)$$

$G_0$  and  $h$  are material properties,  $e$  is the void ratio and  $P_a$  is the atmospheric pressure. The bulk modulus may be computed by assuming a value for Poisson's ratio. For the soil mass, the overall stress-strain increments relation, to obtain plastic strain increments ( $d\epsilon^p$ ), is expressed as:

$$d\epsilon^p = C^p \cdot d\sigma \quad (6)$$

$C^p$  is plastic compliance matrix. Clearly, it is expected that all effects of plastic behaviour be included in  $C^p$ . To find out  $C^p$ , the constitutive equations for a typical slip plane must be considered in calculations. Consequently, the appropriate summation of all provided compliance matrices corresponding to considered slip planes yields overall  $C^p$ , therefore, strain increment at each stress increment is calculated as follows:

$$d\epsilon^p = \frac{1}{n} \sum_{i=1}^n W_i [L_\epsilon]^T C_i^p [L_\sigma] d\sigma' \quad (7)$$

$L_\epsilon$  and  $L_\sigma$  are transformation matrices for strain and stresses, respectively and  $n$  is number of planes.

## Constitutive Equation for Sampling Points

In many instances, the scale of the microstructure is coarse enough to be out of the range of such specific considerations of slip theory, and the individual component blocks can be considered as a continuum with well-defined plastic resistances and hardening behaviour. In this research, the individual component blocks of the overall media deform collectively as a heterogeneous (but compatible in deformations with other blocks) assembly of continua, interacting with each other only through the boundary conditions applicable at their various interfaces. Figure 1 shows these defined planes (say 13). This number may be chosen as any number, however, based on some numerical experiences 13 is found to fit a rationally justified and posses enough power to show any distribution through the material.

To satisfy conditions of applicability of the theory from the engineering viewpoint, and also to reduce the extremely high computational costs, a limited number of necessary and sufficient sampling planes are considered.

The choice of 13 independent planes (Figure 1) for the solution of any three dimensional problem based on getting a good distribution of plastic deformation through the media and avoiding huge computing time is a fair number. The orientation of the sampling planes as given by their direction cosines of normal axis and the weight coefficients for numerical integration rule are given in fist three and the last rows of Table 1. The coefficients  $W_i$  choosing any number of sampling points, are simply calculated based on Gauss quadrature numerical integration rule.

A coordinate system has been employed for each plane in such manner that one axis is perpendicular to the plane and the other two are laid on the plane. Plastic shear strain increments on each plane is considered as two component vectors on defined coordinate axes of plane. The presented  $W_i$  are

acceptable for a first order tensor. They must be corrected for a second order tensor like stress or strain distribution over the surface of sphere. They must be multiplied by the ratio of area for each sampling plane on sphere.

**Table 1:** Cosines of normal axis and the weight coefficients for numerical integration

Plane NO		1	2	3	4	5	6	7	8	9	10	11	12	13
NORMAL AXIS	$l_i$	$\frac{\sqrt{3}}{3}$	$\frac{\sqrt{3}}{3}$	$-\frac{\sqrt{3}}{3}$	$-\frac{\sqrt{3}}{3}$	$\frac{\sqrt{2}}{2}$	$-\frac{\sqrt{2}}{2}$	$\frac{\sqrt{2}}{2}$	$-\frac{\sqrt{2}}{2}$	0	0	1	0	0
	$m_i$	$\frac{\sqrt{3}}{3}$	$-\frac{\sqrt{3}}{3}$	$\frac{\sqrt{3}}{3}$	$-\frac{\sqrt{3}}{3}$	$\frac{\sqrt{2}}{2}$	$\frac{\sqrt{2}}{2}$	0	0	$-\frac{\sqrt{2}}{2}$	$\frac{\sqrt{2}}{2}$	0	1	0
	$n_i$	$\frac{\sqrt{3}}{3}$	$\frac{\sqrt{3}}{3}$	$\frac{\sqrt{3}}{3}$	$\frac{\sqrt{3}}{3}$	0	0	$\frac{\sqrt{2}}{2}$	$\frac{\sqrt{2}}{2}$	$\frac{\sqrt{2}}{2}$	$\frac{\sqrt{2}}{2}$	0	0	0
$W_i$		$\frac{27}{840}$	$\frac{27}{840}$	$\frac{27}{840}$	$\frac{27}{840}$	$\frac{32}{840}$	$\frac{32}{840}$	$\frac{32}{840}$	$\frac{32}{840}$	$\frac{32}{840}$	$\frac{32}{840}$	$\frac{40}{840}$	$\frac{40}{840}$	$\frac{40}{840}$

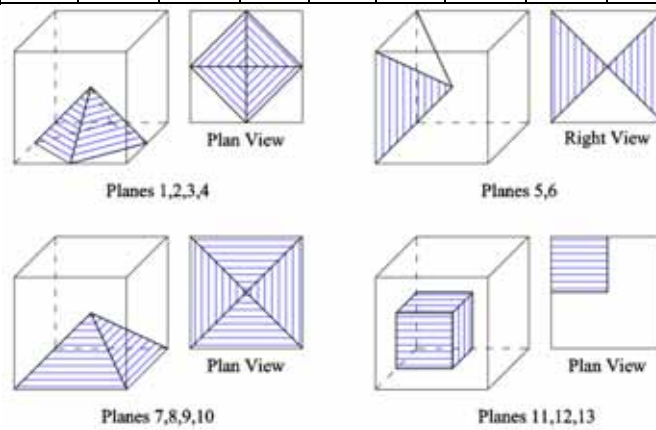


**Figure 1:** Definition of 13 planes.

### STRESS AND STRAIN VECTORS

In all that follows  $\{ \}$  denotes a (9) 6-element column vector and  $[ ]$  a matrix. The superscript T indicates the transposed array. A superposed dot indicates the rate,  $u(\cdot)$  is the Heaviside step function ( $u(x > 0) = 1$  and  $u(x \leq 0) = 0$ ),  $\langle \rangle$  are the Macaulay brackets ( $\langle x \rangle = u(x) \cdot x$ ) and  $| \cdot |$  refers to the norm. Following this notation  $\| \{ \} \|$  is the length of a vector whereas  $\{ \cdot \}$  represents a Unit vector ( $\{ \cdot \} = \{ \} / \| \{ \} \|$ ). A comma followed by a subscripted variable implies the partial derivative with respect to that variable. Bars over the stress quantities refer to points on the bounding surface (or the yield surface in conventional plasticity theory). The effective stress vector, the strain vector, the vector equivalent of the Kronecker delta tensor are defined as

$$\begin{aligned}
 \{\mathcal{E}\} &= \{\varepsilon_{11} \quad \varepsilon_{22} \quad \varepsilon_{33} \quad \varepsilon_{12} \quad \varepsilon_{21} \quad \varepsilon_{13} \quad \varepsilon_{31} \quad \varepsilon_{23} \quad \varepsilon_{32}\}^T \\
 \{\mathcal{S}\} &= \{\sigma_{11} \quad \sigma_{22} \quad \sigma_{33} \quad \sigma_{12} \quad \sigma_{21} \quad \sigma_{13} \quad \sigma_{31} \quad \sigma_{23} \quad \sigma_{32}\}^T \\
 \{\mathcal{D}\} &= \{1 \quad 1 \quad 1 \quad 0 \quad 0 \quad 0 \quad 0 \quad 0 \quad 0\}^T
 \end{aligned} \tag{8}$$

The stress vector is transferred on all planes to establish the plasticity of each one. These transfers are done by multiplying related transitive matrixes which are derived from their direction cosines. There are three stress components, first one is normal  $\sigma_n$  and others  $\tau_1$  and  $\tau_2$  are tangential, on each plane.

$$\begin{Bmatrix} \tau_1 \\ \tau_2 \\ \sigma_n \end{Bmatrix}_i = [T_i] \cdot \{\sigma\}, \quad \tau = \sqrt{\tau_1^2 + \tau_2^2} \quad (9)$$

$[T_i]$  is the transitive matrix of plane  $i$  and defined as:

$$[T_i] = \begin{bmatrix} L_{x'_ix} & L_{x'_iy} & L_{x'_iz} \\ L_{y'_ix} & L_{y'_iy} & L_{y'_iz} \\ L_{z'_ix} & L_{z'_iy} & L_{z'_iz} \end{bmatrix} \cdot \begin{bmatrix} l_i & 0 & 0 & m_i & 0 & n_i & 0 & 0 & 0 \\ 0 & m_i & 0 & 0 & l_i & 0 & 0 & n_i & 0 \\ 0 & 0 & n_i & 0 & 0 & 0 & l_i & 0 & m_i \end{bmatrix} \quad (10)$$

Based on description of local axes, and also the relations for transition of stress tensor to an arbitrary plane, we must multiply the transferred matrix by a rotation matrix to be presented in our local axes on each plane. Therefore,  $L$  is the rotation matrix, and  $x'_i$ ,  $y'_i$  and  $z'_i$  are local axes of plane  $i$  and

$$\begin{aligned} S_{x_i} &= l_i \cdot \sigma_{11} + m_i \cdot \sigma_{12} + n_i \cdot \sigma_{13} \\ S_{y_i} &= l_i \cdot \sigma_{21} + m_i \cdot \sigma_{22} + n_i \cdot \sigma_{23} \\ S_{z_i} &= l_i \cdot \sigma_{31} + m_i \cdot \sigma_{32} + n_i \cdot \sigma_{33} \end{aligned} \quad (11)$$

$S_{x_i}$ ,  $S_{y_i}$  and  $S_{z_i}$  are stress component of plane  $i$  in global directions. Then, the derivatives of  $\sigma_n$  and  $\tau$  are:

$$\sigma_{n,\sigma_i} = \begin{Bmatrix} l_i \cdot l_i \\ m_i \cdot m_i \\ n_i \cdot n_i \\ m_i \cdot l_i \\ m_i \cdot l_i \\ n_i \cdot l_i \\ n_i \cdot l_i \\ n_i \cdot m_i \\ n_i \cdot m_i \end{Bmatrix}, \quad \tau_{,\sigma_i} = \left( \frac{1}{\tau} \right) \cdot \begin{Bmatrix} S_{x_i} \cdot l_i - \sigma_n \cdot l_i^2 \\ S_{y_i} \cdot m_i - \sigma_n \cdot m_i^2 \\ S_{z_i} \cdot n_i - \sigma_n \cdot n_i^2 \\ S_{x_i} \cdot m_i - \sigma_n \cdot m_i \cdot l_i \\ S_{y_i} \cdot l_i - \sigma_n \cdot m_i \cdot l_i \\ S_{x_i} \cdot n_i - \sigma_n \cdot n_i \cdot l_i \\ S_{z_i} \cdot l_i - \sigma_n \cdot n_i \cdot l_i \\ S_{y_i} \cdot n_i - \sigma_n \cdot n_i \cdot m_i \\ S_{z_i} \cdot m_i - \sigma_n \cdot n_i \cdot m_i \end{Bmatrix} \quad (12)$$

In the relations related to different planes, stress components obtained from planes are not always equal to the projection of the stress tensor, and only they are equivalent in the unique condition [7]. However, generally the stress components on each plane are independent. It suffices to say that this deficiency does not produce significant error which can be omitted by calibration. The best way to avoid this problem is using virtual work rule [8]. Also, stress ratio of each plane defined as follows

$$\zeta = \frac{\tau}{\sigma_n} \quad (13)$$

## BOUNDING SURFACE PLASTICITY

The strain rate is sum of elastic and plastic components:

$$\{\dot{\epsilon}\} = \{\dot{\epsilon}^e\} + \{\dot{\epsilon}^p\} \quad (14)$$

The superscripts e and p refer to the elastic and plastic parts. The recent relation can be presented as:

$$\begin{aligned} \{\dot{\epsilon}\} &= [C^e]_T \cdot \{\dot{\sigma}\} + [C^p]_T \cdot \{\dot{\sigma}\} \\ [C^{ep}]_T &= [C^e]_T + [C^p]_T \end{aligned} \quad (15)$$

And for each plane:

$$[C^e]_i = \frac{1}{2G_i} [I] + \left( \frac{1}{9K_i} - \frac{1}{6G_i} \right) \cdot \{\delta\} \cdot \{\delta\}^T, \quad [C^p]_i = \frac{1}{H_i} \{Q\}_i \cdot \{P\}_i^T \quad (16)$$

$[C^e]_T$  and  $[C^p]_T$  are obtained from following relation based on accumulating quotas of planes:

$$\begin{aligned} [C^p]_T &= 8\pi \cdot \sum_{i=1}^{13} w_i \cdot [C^p]_i \\ [C^e]_T &= 8\pi \cdot \sum_{i=1}^{13} w_i \cdot [C^e]_i \end{aligned} \quad (17)$$

On the grounds that the elastic dominion is small in soils, the elasticity parameters (Bulk and shear modules) in this model comply with the average of principal stresses, and also to avoid extra calculations, in the multi-laminate model elastic behavior is considered as isotropic one for all planes. In other words, the  $[C^e]$  can be present only for the main point; thus, only the plastic behavior of the material (i.e.  $[C^p]_T$ ) comes from numerical integration of the plastic treatment of planes (i.e.  $[C^p]_i$ ):

$$[C^{ep}]_T = [C^e]_T + [C^p]_T \quad (18)$$

For each plane, the model needs to define four surfaces in effective stress space (i) the failure surface to define the critical-stress state. (ii) The bounding surface  $F$ , to record the limit of previous loading, to help construct the loading surface and to determine the bounding plastic modulus  $\bar{H}$ . (iii) The loading surface  $f$ , to determine the direction of plastic loading  $\{Q\}$  (which is also used to determine the direction of the deviatoric plastic strain rate) and the additive plastic modulus  $H_f$ . (iv) The plastic dilatancy surface  $g$ , (similar to a plastic potential surface) which determines the ratio of the volumetric to deviatoric plastic strain rates.

## BOUNDING SURFACE

Three segments are constructed meridional sections of the isotropic bounding surface (i) a compressive ellipse, (ii) a hyperbola and (iii) a tensile ellipse (Figure 2). This form was originally proposed by Dafalias and Herrmann [2]. The compressive elliptic part lies in  $\sigma_{m1} \leq \sigma_n \leq \sigma_{n0}$  region where  $\sigma_{m1} = \sigma_{n0}/R$ .  $R$  is a material constant ( $1 \leq R < \infty$ ).  $\sigma_{n0}$  varies as a function of the volumetric plastic strain and defines the size of bounding surface. The compressive ellipse meets the normal stress axis perpendicularly. The equation of the first part is given as

$$F = \bar{\tau} - \frac{N \cdot \sigma_{n0}}{R} \sqrt{\left(1 - \left(\frac{R\bar{\sigma}_n / \sigma_{n0}}{R-1} - 1\right)^2\right)} = 0 \quad (19)$$

$N$  is slope of the line which passes from common tangent point of ellipse and hyperbola. The common tangent is parallel to normal stress axis. The hyperbola is located in  $\sigma_{n2} < \sigma_n < \sigma_{n1}$  region and defined as

$$F = \bar{\tau} - \frac{N \cdot \sigma_{n0}}{R} \left(1 + \frac{AR}{N} - \sqrt{\left(1 - \frac{R\bar{\sigma}_n}{\sigma_{n0}}\right)^2 + \left(\frac{AR}{N}\right)^2}\right) = 0 \quad (20)$$

$A \cdot \sigma_{n0}$  manipulates the gap between N-line and the asymptote to the hyperbolic segment, which is parallel to the N-line.

The last part is a tensile ellipse situated in  $\sigma_{n3} \leq \sigma_n \leq \sigma_{n2}$  where  $\sigma_{n3} = T \cdot \sigma_{n0}$ , and  $\sigma_{n2} = D \cdot \sigma_{n0}$ , and it is proposed as

$$F = \bar{\tau} - \tau_r \sqrt{\left(1 - \left(1 - \frac{\bar{\sigma}_n - T\sigma_{n0}}{\sigma_{nr}}\right)^2\right)} = 0 \quad (21)$$

$$\sigma_{nr} = \frac{(D\sigma_{n0}/R) + \sigma_{n0}(\Psi/\tau_2)(T^2 - (D/R)^2)}{1 + 2\sigma_{n0}(\Psi/\tau_2)(T - (D/R))} \quad (22)$$

$$\tau_r = \frac{\tau_2}{\sqrt{\left(1 - \left(1 - \frac{(D\sigma_{n0}/R) - T\sigma_{n0}}{\sigma_{nr}}\right)^2\right)}} \quad (23)$$

$$\Psi = \frac{N \cdot (1 - D)}{\sqrt{\left((1 - D)^2 + (AR/N)^2\right)}} \quad (24)$$

$$J_2 = \frac{N \cdot \sigma_{n0}}{R} \left(1 + \frac{AR}{N} - \sqrt{\left((1 - D)^2 + (AR/N)^2\right)}\right) \quad (25)$$

$D$  is zero in this paper; namely,  $\sigma_{n2} = 0$ . Moreover, the length of tensile cut-off is defined by  $\sigma_{n3}$ . When  $D = 0$ ,  $T$  must lie in  $-J_2/2\Psi\sigma_{n0} \leq T \leq 0$  (the average amount of this range is recommended).

## CRITICAL STATE LINE, NORMAL CONSOLIDATION LINE AND REBOUND LINES

In this model, the critical state, normal consolidation, and rebound lines are defined similar to what Crouch et al. [10] defined by the exception that here the space is  $e - Ln\sigma_n$  instead of  $e - LnI/3$ . Finally, the passing line from intersection of compressive ellipse, and hyperbola segments is obtained as:

$$N = \frac{A - \zeta_{cr} \left( \frac{\sigma_{cr}}{\sigma_{n_0}} \right) - \sqrt{\left( \left( \zeta_{cr} \cdot \left( \frac{\sigma_{cr}}{\sigma_{n_0}} \right) - A \right)^2 - \zeta_{cr} \cdot R \cdot \left( \frac{\sigma_{cr}}{\sigma_{n_0}} \right)^2 \left( R \cdot \left( \frac{\sigma_{cr}}{\sigma_{n_0}} \right) - 2 \right) \cdot \left( 2A - \zeta_{cr} \cdot \left( \frac{\sigma_{cr}}{\sigma_{n_0}} \right) \right) \right)}}{\left( \frac{\sigma_{cr}}{\sigma_{n_0}} \right) \cdot \left( R \cdot \left( \frac{\sigma_{cr}}{\sigma_{n_0}} \right) - 2 \right)} \quad (26)$$

## HARDENING/SOFTENING EQUATION

The most crucial hardening/softening parameter is  $\dot{\sigma}_{n_0}$  which defines the size of bounding surface (the intersection of compressive ellipse with normal stress axis). Variation in the amount of this parameter is a function of volumetric plastic strain as follows:

$$\dot{k} = \dot{\sigma}_{n_0} = \frac{\langle \sigma_{n_0} - \sigma_l \rangle + \sigma_l}{\lambda + \kappa} (1 + e_{in}) \cdot \dot{\epsilon}_v^p \quad (27)$$

Moreover, elastic behavior of the model is not linear, and is a function of confinement pressure. As said, elastic behavior is not transferred to planes, so the Bulk modulus complies from the hyper elastic formulation:

$$K = \frac{(1 + e_{in}) \cdot (\langle P - \sigma_l \rangle + \sigma_l)}{\kappa} \quad (28)$$

$P$  and  $\sigma_l$  are the average amount of principal stresses at the point, and model constant, respectively.  $\sigma_l$  represents a limitation that there is no effect on bulk and shear modules when  $P$  is lower than it. By assuming constant Poisson's ratio  $\nu$  tangent shear modulus can be defined as:

$$G = \frac{1.5K(1 - 2\nu)}{1 + \nu} \quad (29)$$

## LOADING SURFACE

The model introduces an innovative approach to define the loading surface  $f$  by using deviatoric and radial mapping rules. This surface always passes through the stress point and by defining an image point on the bounding surface the similarity ratio can be determined. The radial mapping rule is applied for the compressive ellipse part where the projection centre located at  $C\sigma_{n_0}$  on the  $\sigma_n$  axis.  $C$  assumes the value  $1/R$  in the following. When  $\sigma < \sigma_{n_0}/R$ , the model uses deviatoric mapping rule to construct the loading

surface whereas the current stress point and image point on bounding surface have the same  $\sigma_n$ . If  $\tau > 0$  then the similarity ratio is defined as

$$\beta = \frac{\bar{\tau}}{\tau} \quad (30)$$

However, for points on the  $\sigma_n$  axis and  $\sigma_n > \sigma_{n0}/R$  this ratio is determined by

$$\beta = \frac{\sigma_{n_0} \cdot \left(\frac{1}{R} - 1\right)}{\frac{\sigma_{n_0}}{R} - \sigma_n} \quad (31)$$

A plastic behavior takes place during loading along  $\sigma_n$  axis in the radial mapping, while a completely elastic response happens during loading along  $\sigma_n$  axis in the deviatoric mapping region ( $\tau = 0$  and  $\beta = \infty$ ). Therefore, the loading surface equation in the radial mapping region is defined by substituting  $(\sigma_{n0}/R) + \beta(\sigma_n - (\sigma_{n0}/R))$  for  $\bar{\sigma}_n$  and  $\beta\tau$  for  $\bar{\tau}$ :

$$f = \beta\tau - \frac{N \cdot \sigma_{n_0}}{R} \sqrt{\left(1 - \left(\frac{\beta(R\sigma_n/\sigma_{n_0} - 1)}{R-1}\right)^2\right)} = 0 \quad (32)$$

In the presented model, owing to the fact that model works with normal and shear stresses instead of stress invariants, model is able to consider the rotation of principal stresses. The related functions are, thus, specified after substituting  $\sigma_n$  for  $\bar{\sigma}_n$  and  $\beta\tau$  for  $\bar{\tau}$  as follows in deviatoric mapping region instead of utilizing complicated movement rules of projection center:

$$f = \beta\tau - \frac{N \cdot \sigma_{n_0}}{R} \left(1 + \frac{AR}{N} - \sqrt{\left(\left(1 - \frac{R\sigma_n}{\sigma_{n_0}}\right)^2 + \left(\frac{AR}{N}\right)^2\right)}\right) = 0 \quad (33)$$

$$f = \beta\tau - \tau_r \sqrt{\left(1 - \left(1 - \frac{\sigma_n - T\sigma_{n_0}}{\sigma_{n_r}}\right)^2\right)} = 0 \quad (34)$$

Now, by defining loading surface it is easy to obtain direction of plastic loading

$$\{Q\} = \frac{\{f, \sigma\}}{\{f, \sigma\}} = Q_v \cdot \{\delta\} + \{Q_s\} \quad (35)$$

$$\{Q\} = \frac{1}{\{f, \sigma\}} \cdot \left( \underbrace{f, \sigma_n \cdot \{\sigma_n, \sigma\}}_{hydrostatic} + \underbrace{f, \tau \cdot \{\tau, \sigma\}}_{deviatoric} \right) \quad (36)$$

The deviatoric part  $\{Q_s\}$  is, then, utilized to obtain the direction of plastic strain in later sections.

## PLASTIC DILATANCY SURFACE AND PLASTIC STRAIN DIRECTION

The form of this surface is akin to bounding surface with its three segments; however, the squared terms for compressive ellipse are replaced by  $n_g$  ( $2 < n_g < \infty$  for super-ellipse and  $1 < n_g < 2$  for sub-ellipse). The plastic surface, as a result, is obtained as

$$g = \tau - \frac{N_g \cdot \sigma_{n0g}}{R_g} \cdot \left( 1 - \left( \frac{(R_g \sigma_n / \sigma_{n0g} - 1)}{R_g - 1} \right)^{n_g} \right)^{\frac{1}{n_g}} = 0 \quad (37)$$

$N_g, R_g$  and  $\sigma_{n0g}$  have the identical concepts as  $N, R$  and  $\sigma_{n0}$  for the bounding surface. Note that  $\sigma_{n0g}$  is scaled until the dilatancy surface passes through the current stress point.

There are three important notes about plastic dilatancy surface:

- (i) The compressive ellipse meets the normal stress axis perpendicularly. This is, in this point all amounts of plastic strain are volumetric.
- (ii) The common tangent of Hyperbola and Compressive ellipse segments is parallel to normal stress axis. In other words, in this point all amounts of plastic strain are deviatoric.
- (iii)  $N_g = \zeta_{cr}$ , this means that the vertex of the plastic dilatancy surface (intersection of compressive ellipse and hyperbola) is met by critical state line, where the horizontal projection of plastic strain direction is zero; thus, all amounts of plastic strain are deviatoric.

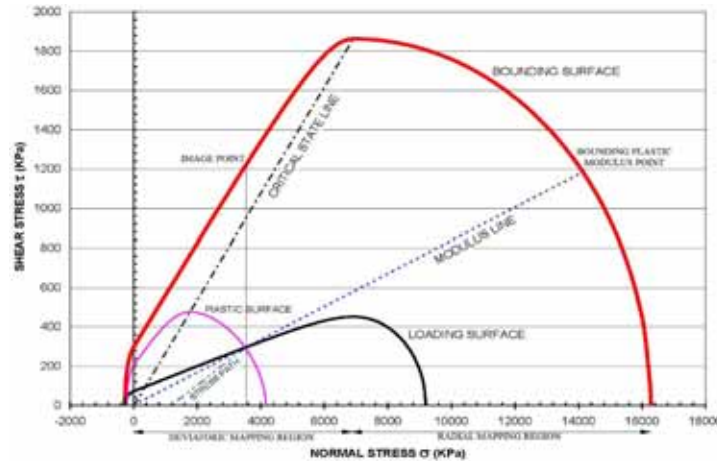


Figure 2: Definition of the different surfaces in  $\tau - \sigma$  space.

Despite the fact that the shape of bounding surface and plastic dilatancy surface are similar, flow rule is non-associated, as bounding surface and loading surface are not geometrically similar by virtue of the mapping rules. Then the direction of the plastic strain rate is obtained as:

$$\{P\} = \frac{1}{\{g_{,\sigma}\}} \cdot (g_{,\sigma_n} \cdot \{\sigma_{n,\sigma}\} + f_{,\tau} \cdot \{\tau_{,\sigma}\}) \quad (38)$$

## BOUNDING AND ADDITIVE PLASTIC MODULI

The bounding plastic modulus point is a point on the bounding surface and it has the same  $\zeta$  with the current stress point. To define this point, we can draw a line from origin to the current stress point and continue until it intersects the bounding surface.

After substituting equation (46) into hardening rule, the variable  $V$  is computed as:

$$V = \frac{\langle \sigma_{n_0} - \sigma_l \rangle + \sigma_l}{\lambda - \kappa} (1 + e_{in}) \{\delta\}^T \{P\} \quad (39)$$

$$\frac{1}{\bar{H}} = - \frac{\{F_{,\bar{\sigma}}\}}{F_{,\sigma_{n_0}} \cdot V} \quad (40)$$

By balancing the last two equations, the bounding plastic modulus is obtained as

$$\bar{H} = - \frac{\langle \sigma_{n_0} - \sigma_l \rangle + \sigma_l}{\lambda - \kappa} \cdot (1 + e_{in}) \frac{F_{,I_0}}{\{F_{,\bar{\sigma}}\}} \{\delta\}^T \{P\} \quad (41)$$

Where  $F_{,I_0}$  and  $\{F_{,\bar{\sigma}}\}$  are calculated at the bounding plastic modulus. In addition, proximity-dependent additive plastic modulus can be defined as

$$H_f = \frac{\langle \sigma_{n_0} - \sigma_l \rangle + \sigma_l}{\lambda - \kappa} \cdot (1 + e_{in}) \frac{h}{\langle \beta / (\beta - 1) - s \rangle^{n_H}} \left( \frac{\langle \sigma_{n_0} - \sigma_l \rangle + \sigma_l}{\sigma_{at}} \right)^{z_0} \quad (42)$$

$h$ ,  $s$  and  $\sigma_{at}$  are shape hardening factor, ratio of the size of elastic kernel and atmosphere pressure, respectively. Moreover,  $z_0$  and  $n_H$  are material constants.

Generally,  $s$  defines a elastic zone enclosing the projection centre.  $z_0$  shows the importance of a stiffer behavior for denser states, and  $n_H$  controls the rate at which the additive plastic modulus falls with respect to the proximity of the current stress point to its image point on the bounding surface. The shape hardening parameter which has a strong effect on behavior of the model for stress paths inside the bounding surface is derived by  $h_1$  and  $h_2$  which are the coincident amounts of  $\sigma_{n_1} = \sigma_{n_0} / R$  and  $\sigma_{n_2} = 0$ .

$$h = \left( h_1 - \left\langle 1 - \frac{\sigma_n R}{\sigma_{n_0}} \right\rangle \cdot (h_1 - h_2) \right) \cdot \left( 1 + z_1 \left\langle 1 - \left( \frac{\tau}{\max(\tau)} \right)^{z_2} \right\rangle \right) \quad (43)$$

$z_1$  and  $z_2$  are the material constants, and  $\max(\tau)$  is the maximum quantity of shear stress along the stress path. Finally, Figure 3 shows the flow chart that how the model acts.

## MODEL PARAMETERS

Firoozkoh sand has been chosen to be the soil type 1 in sand box. Upon a few triaxial standard tests the model parameters provided and are presented in Table 2.

**Table 2:** Model parameters

Critical state line slope in $e - \ln(I/3)$ space	: $\lambda$
Changed value of critical state line slope in $e - \ln(I/3)$ space at $e_{crk}$	: $\lambda_L$
Parameter for size of boundary surface	: $A_c$
Parameter for size of boundary surface of plastic potential	: $A_{gc}$
Shape hardening parameter	: $h_{1c}$
Ratio of normal stresses boundary surface and compression and hyperbolic ellipsoid	: $R$
Poisson ratio	: $\nu$
Power in compression ellipse of plastic potential	: $n_g$
Unloading line slope	: $\kappa$
Initial void ratio	: $e_{in}$
Critical state line slope in $\tau \sim \sigma_n$ space	: $\zeta_{cr_c}$
Initial mean stress	: $P_o$
Void ratio of critical state line slope in $e - \ln(I/3)$ space at $e_{crk}$	: $e_{cr_k}$

## STRENGTH ELLIPSOID

In general, quantitative description of initial micro-fabric (bedding plane effects) would enhance characterization and forecasting of sand behaviour under different loading. On loading the fabric is continuously altered. Hence, it is necessary to develop techniques to quantify the changes in fabric as well. While the material is distorted the fabric of the material changes and so there is the strain or displacement field in the material. Consequently, the strain and induced fabric of a material are inherently related to each other.

A popular approach for formulation of strength criteria for anisotropy granular materials is the generalization of isotropic ones. Such a criterion is usually geometrically interpreted as a limiting envelope in a stress space; which means that a condition of failure occurs when a given stress vector touches the failure envelope. Since the condition for failure is intrinsic to the material, the failure criterion can be defined differently for any probable sliding plane through material. Accordingly, the stress ratio cannot exceed the corresponding value of  $(\tan(\varphi))$  on neither on the planes of weakness nor on any other plane which not tending to slide.

On a loading orientation inclined by three angles (direction cosines) respect to the bedding plane, a certain sliding mechanism composed of active sliding planes provide a value of stress ratio which corresponds to the most active plane and has a limitation of  $(\eta_c \tan(\varphi))$  or  $\zeta_{cr_c}$ , while  $0 < \eta_c < 1$ ) that is governing sand strength representative against sliding. Therefore, on any orientation within the sand, the state of strength depends on the geometry of bedding plane and the orientation of applied load with respect to bedding plane. To describe the strength representative,  $(\zeta_{cr_c})$ , at any orientation, it is needed to find a way of summarizing the configuration of different strengths corresponding to all of probable directions passing through the medium.

For ideal granular media with no preferential orientation a spherical envelop of strength representatives ( $\zeta_{\text{crc}}$ ) may provide uniform sliding strength on any orientation. However, to consider fabric effects due to bedding plane, an ellipsoidal envelop of strength may be the most suitable presentation of strength variation on different directions. The longest diameter of this ellipsoid is always normal to bedding plane. Configuring the 13 predefined planes in strength ellipsoid provides a certain elliptical section on each plane that present the variation of strength with respect to sliding orientation. In other words, the tips of the arrows head of strength value of different orientations, collectively define a built up geometrical surface called the strength ellipsoid. Obviously, the size of strength ellipsoid of each plane is different and present maximum and minimum strengths for sliding along the longest and shortest ellipse respectively. The other sliding orientations are faced on strength limitations in between depend on the direction of shear stress on plane respect to bedding plane.

Adopting the multi-plane mechanism of sliding planes configured in Figure 1 with respect to orientation of applied major principal stress axis, these planes are configured in symmetric manner around major principal axis. Any change in principal stress axis direction creates a new set of strength ellipses with different strength against sliding directions on different planes.

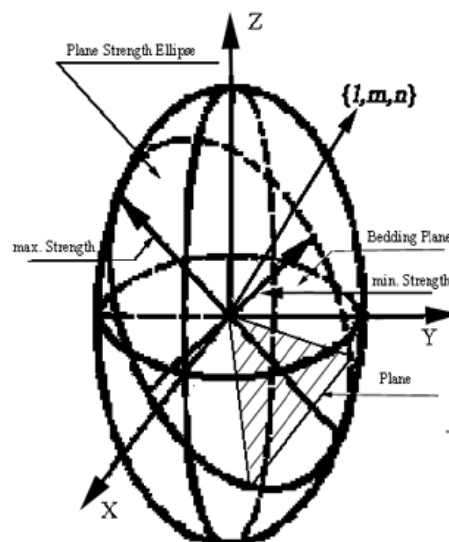


**Figure 3:** Typical ellipse strength of a plane in ellipsoid strength (Embedded plane assumed to be horizontal)

This study carried out for micro-fabric behaviour of loose, medium, and dense granular materials led to the establishment of a statistical criterion of natural anisotropy based on hypotheses that experience accepted as probable. The fabric anisotropy law is represented as a spatial closed ellipsoid strength function in  $x$ ,  $y$ , and  $z$  coordinates as follows:

$$x^2 / B + y^2 / B + z^2 / A - 1 = 0 \quad (44)$$

$A$ ,  $B$ , and  $C$  are three mutually perpendicular diameters of ellipsoid respectively. A construction of typical ellipsoid is shown in Figure 3.

Furthermore, to overcome the anisotropy concerns the loading orientation, a possible having all different probable sliding mechanisms must be provided in the used model. In this way, application of any arbitrary loading or stress path leads to a certain sliding mechanism obeys the minimum energy level in natural law. These possibilities are provided in an elastic-plastic Multi-Plane model.

To find the strength ellipsoid diameters, two triaxial standard compression tests must be arranged; one with horizontal bedding plane and vertical loading axis (test one), and the other with both vertical bedding plane and loading axis (test two). According to author experience [26], in both of two tests planes 1 to 4 are mostly active, however, in the second case because of 90 degree rotation of load in axis, the smaller ellipse of strength on active planes are provided by the main strength ellipsoid. There less friction angles are applicable while loading axis diverged respect to normal axis to bedding plane. In triaxial compression test, the sliding orientation on active planes is along the longest diameter of each plane strength ellipse. Furthermore, these four most activated planes in test one is symmetrically located around loading axis that is identical with normal line to bedding plane. Therefore, for any axe-symmetry loading conditions similar to triaxial compression test, there should be axe-symmetry of strength respect to normal axis to bedding plane. In this case, the obtained  $\zeta_{\text{crc}}$  value from test and the coordinates of tip head arrows of shear strain on planes provide a unique equation relates the unknown strength ellipsoid parameters. However, due to axi-symmetry, two minor diameters of strength ellipsoid are equal, so,  $B=C$ . To find the coordinates of tip head arrows of shear strain, one simply can obtain direction cosines of shear stress/strain on corresponding plane, considering the length of arrow to be equal to  $\zeta_{\text{crc}}$ , one point of strength ellipsoid is known. It must be added that in triaxial standard tests, the coaxiality of strain and stress is valid, therefore, to obtain any active plane sliding that is enough to find the direction of corresponding shear stress. In second compression test, the loading axis is rotated by 90 degree, so, the same active planes rotated by same angle and their strength ellipses as well. In this case, the geometry of strength ellipsoid is the same as test one. However, different  $\zeta_{\text{crc}}$  and coordinates of tip head arrows are provided that lead to provide the second relation between strength ellipsoid parameters. The simultaneous solution of both equations presents the unknown parameters  $A$ ,  $B$ , and  $C$ . Assuming the direction cosines of the advanced active planes in first and second tests as  $\ell, m, n$  and  $\ell', m', n'$ , respectively,  $A$  and  $B$  are calculated as follows:

$$\begin{aligned} x_1^2 + y_1^2 + z_1^2 &= \zeta_{\text{crc}}^2, \\ x_1'^2 + y_1'^2 + z_1'^2 &= \zeta_{\text{crc}}'^2 \end{aligned} \quad (45)$$

$$\begin{aligned} \frac{\ell^2 \zeta_{\text{crc}}^2}{B^2} + \frac{m^2 \zeta_{\text{crc}}^2}{B^2} + \frac{n^2 \zeta_{\text{crc}}^2}{A^2} &= 1, \\ \frac{(\ell' \zeta_{\text{crc}}')^2}{B^2} + \frac{(m' \zeta_{\text{crc}}')^2}{B^2} + \frac{(n' \zeta_{\text{crc}}')^2}{A^2} &= 1 \end{aligned} \quad (46)$$

The simultaneous solution of two equation yields:

$$A = \frac{\sqrt{(\ell^2 + m^2)n^2 - n^2(\ell'^2 + m'^2)} \zeta_{\text{crc}} \zeta_{\text{crc}}'}{\sqrt{(\ell^2 + m^2) \tan^2(\varphi) - (\ell'^2 + m'^2)} \zeta_{\text{crc}}'^2} \quad (47)$$

$$B = \frac{\sqrt{(\ell^2 + m^2)n^2 - n^2(\ell'^2 + m'^2)} \zeta_{\text{crc}} \zeta_{\text{crc}}'}{\sqrt{n^2 \zeta_{\text{crc}}^2 - n'^2 \zeta_{\text{crc}}'^2}} \quad (48)$$

Performing a compression plane stress, axe-symmetry condition is not available any more. Prevention of out of plane strain affects the activation and sliding orientation of planes. In this case, conservation of the minimum level of energy law forces the mechanism to occur in different manner as well as geometry. The change in sliding orientation on an active plane from the first natural possible case may make a necessity of grain rolling under constrained conditions. This may lead the sliding to face on local interlocking that generally appears as unstable higher friction angle  $\varphi_f$  that creates an unstable larger

strength ellipsoid for these kinds of sliding planes. This unstable ellipsoid will disappear as soon as the stress path passing over top peak shear strength and softening mode and strength condition comes back to normal strength ellipsoid. Certainly, the larger strength ellipsoid provides a larger unstable intersection strength ellipse on corresponding plane.

To find out the values of internal friction of 13 planes oriented inside a certain strength ellipsoid, first the direction cosines of stress vector as  $\ell'_i, m'_i, n'_i$  are calculated as follows:

$$\beta_i = \arctan \left| \frac{\tau_x}{\tau_y} \right| \quad (49)$$

$$\begin{Bmatrix} \ell'_i \\ m'_i \\ n'_i \end{Bmatrix} = \begin{bmatrix} \cos \beta_i & 0 & -\sin \beta_i \\ 0 & 1 & 0 \\ \sin \beta_i & 0 & \cos \beta_i \end{bmatrix} \begin{Bmatrix} \ell_i \\ m_i \\ n_i \end{Bmatrix} \quad (50)$$

The value of  $\zeta'_{\text{crc}}$  in direction  $\ell'_i, m'_i, n'_i$  is obtained as follows:

$$\zeta'_{\text{crc}} = \frac{A.B}{\sqrt{(\ell_i'^2 + m_i'^2)A^2 + n_i'^2 B^2}} \quad (51)$$

The direction of calculated shear stress on  $i^{\text{th}}$  plane is associated with a certain value of internal friction angle  $\phi_i$  in strength ellipsoid. This friction angle can be obtained through the equation of intersected ellipse plane with strength ellipsoid having the direction of shear stress direction cosines. Simply, any change of shear stresses on planes, is faced on new sliding mechanism and strengths.

## EXPERIMENTAL RESULTS

Figure 5 shows the deviatoric stress and volumetric strain, axial strain in loose sand ( $e_{in} = 0.86$ ) for drained behavior of four loose specimens together with their cell pressures  $\sigma_3$ . The sample under the highest cell pressure undergoes considerable compaction up to 5% for  $\epsilon_v$ , while sample under the lowest cell pressure presents a moderate dilation at 20% axial strain despite being in a loose state. Figure 6 shows the corresponding drained curves for five dense samples  $e_{in} = 0.60$ . The significant dilation up to 12% for  $\epsilon_v$  under low cell pressures is captured well by the model.

## UNDRAINED LOADING

The definition of effective stress for a saturated soil element is stated in macro scale and incremental form as follows:

$$d\sigma = d\sigma' + m \cdot dU \quad (52)$$

$\sigma$  and  $\sigma'$  represent total and effective stresses vectors respectively,  $m$  is constant operator vector equal to  $\{1,1,1,0,0,0\}$ ,  $U$  is the excess pore water pressure, and  $d$  is used for representing small increments.

It can also be assumed that in a fully undrained case, the skeleton volume change is approximately equal to change in the volume of pore water. Defining  $K_f$  as average bulk modulus of soil skeleton,

$$dU = K_f \cdot \{m\}^T d\varepsilon \quad (53)$$

$$\frac{1}{K_f} = \frac{1}{K_w} + \frac{1-\vartheta}{K_s} \quad (54)$$

$K_w$  is bulk modulus of water and  $\vartheta$  is initial porosity. Pore water pressure increment in matrix form is written as follows:

$$dU = K_f \{m\}^T \cdot d\varepsilon \cdot \{m\} \quad (55)$$

Retaining the elastic-plastic constitutive law, it is presented as follows:

$$d\sigma' = D^{ep} \cdot d\varepsilon \quad (56)$$

$$d\sigma = D^{ept} \cdot d\varepsilon \quad (57)$$

The combination of equations 55, 56, and 57 simply result is:

$$D^{ept} = D^{ep} + K_f \cdot \{m\}^T \cdot \{m\} \quad (58)$$

$$D^{ep} = [C^{ep}]^{-1}, \quad C^{ep} = C^e + C^p \quad (59)$$

$C^e$ ,  $C^p$ , and  $C^{ep}$  are compliance elasticity, plasticity, and elastic-plasticity matrices.

According to incremental algorithm,  $C^{ep}$  computed in previous step can be used for current step; therefore, the solution will not remain indeterminate. Consequently,  $D^{ept}$  can be employed to calculate strain increments upon total stress increment tensor.

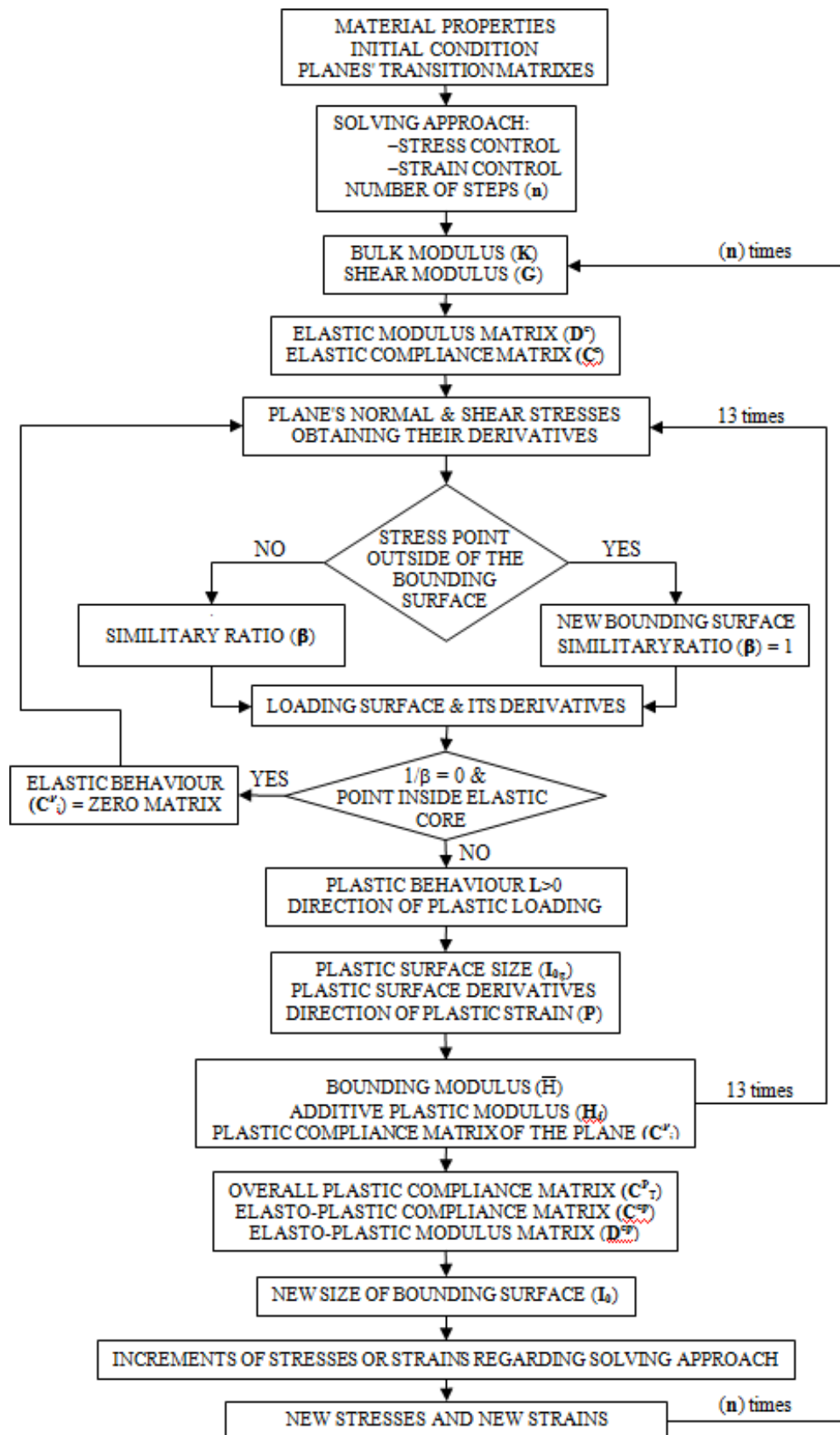


Figure 4: The flow chart of working model

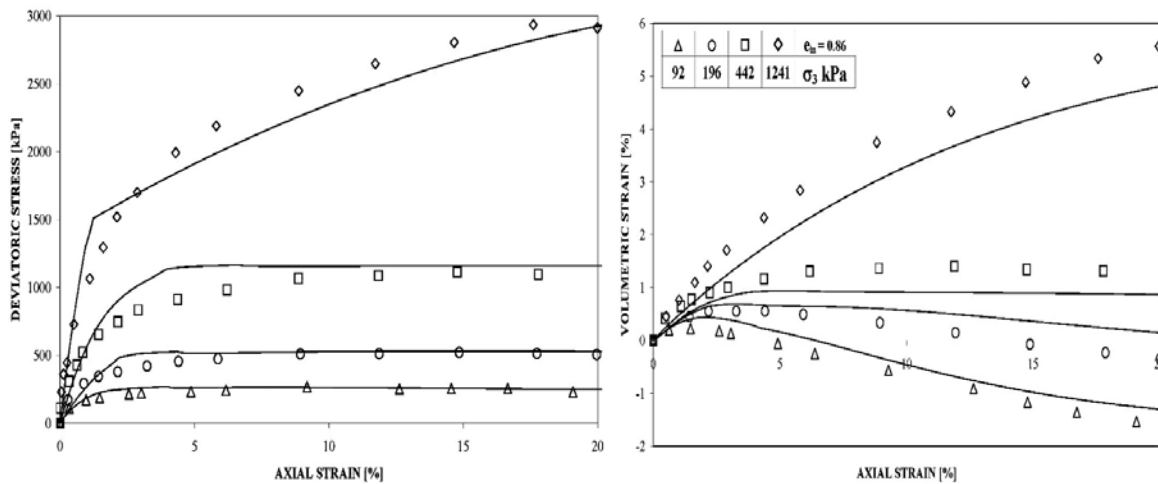


Figure 5: Volumetric strain, and deviatoric stress versus axial strain in loose sand ( $e_{in} = 0.86$ ).

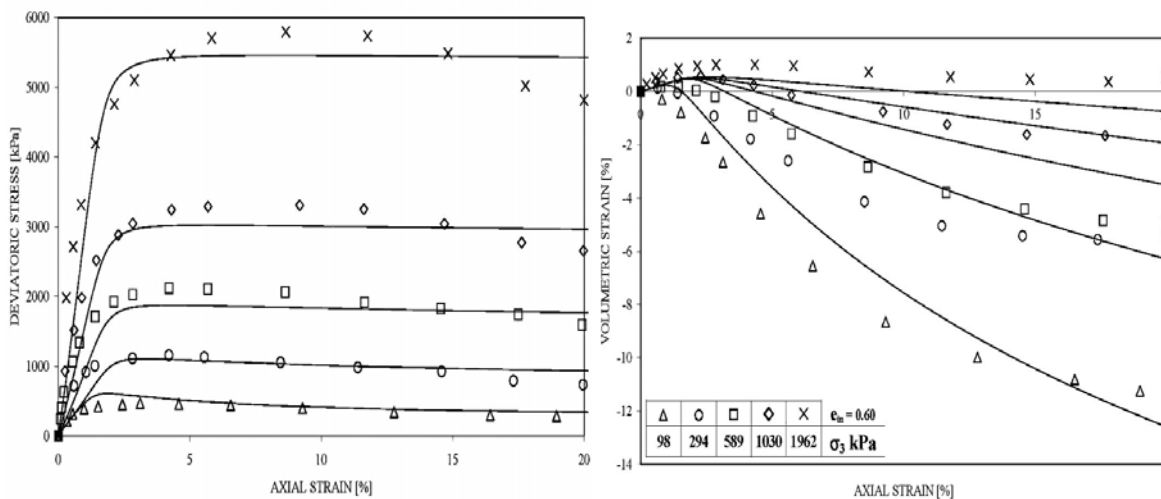


Figure 6: Axial strain versus volumetric strain, and deviatoric stress in loose sand ( $e_{in} = 0.60$ )

### Parameters of Anisotropy

For an axe-symmetry anisotropy of soil that is more practical two triaxial standard compression tests upon horizontal and vertical bedding plane is enough to identify A, B, and C. The strength parameters of multi-plane model are  $\zeta_{crc}$  for 13 planes obtained from the built up strength ellipsoid on corresponding bedding plane for 13 planes as presented in Tables 3 and 4.

The obtained values of  $\zeta_{crc}$  and the ellipsoid parameters A, B, and C are calculated as follows:

**Table 3:** Strength representative ( $\zeta_{crc}$ ) and A, B, and C

Po kPa	90°	0°	A	B	C
50, 200	0.250	0.242	0.06250	0.058564	0.058564

The calculated values of  $\zeta_{crc}$  for different planes and for four embedded plane angles as  $0^\circ$ ,  $30^\circ$ ,  $60^\circ$ , and  $90^\circ$  are presented in Table 3-2.

**Table 4:** The calculated values of  $\zeta_{circ}$ ,  $p=50, 200$  kPa

Plane No.	$\alpha_{\sigma_1}=0^\circ$	$\alpha_{\sigma_1}=30^\circ$	$\alpha_{\sigma_1}=60^\circ$	$\alpha_{\sigma_1}=90^\circ$
1	0.2278	0.2298	0.2298	0.2500
2	0.2278	0.2298	0.2298	0.2500
3	0.2278	0.2258	0.2258	0.2500
4	0.2278	0.2258	0.2258	0.2500
5	0.2408	0.2268	0.2300	0.2500
6	0.2408	0.2268	0.2300	0.2500
7	0.2520	0.2270	0.2500	0.2560
8	0.2520	0.2500	0.2270	0.2560
9	0.2520	0.2310	0.2270	0.2408
10	0.2520	0.2310	0.2290	0.2408
11	0.2400	0.2480	0.2408	0.2408
12	0.2408	0.2260	0.2480	0.2408
13	0.2408	0.2270	0.2298	0.2400

Figure 7-a-1 shows the comparison of model result with tests for  $Po=50$  kPa. and  $a=90, 30$  as stress deviator versus axial strain. Also, corresponding comparison of volumetric strains are shown in Figure 7-a-2. The comparison of the results for  $a=60$ , and  $0$  are shown in Figure 7-b-1, and 2, respectively. Similar sets of the comparison of results in the case of  $Po=200$  kPa. are shown in Figure 8-a-1, 2, and 8-b-1, 2.

To show the capability of model in prediction of results approaching instability conditions in undrained tests, Figure 9-a, b show the comparison of model results with tests in stress paths, deviatoric stress changes versus axial strains for loose and stiff sands.

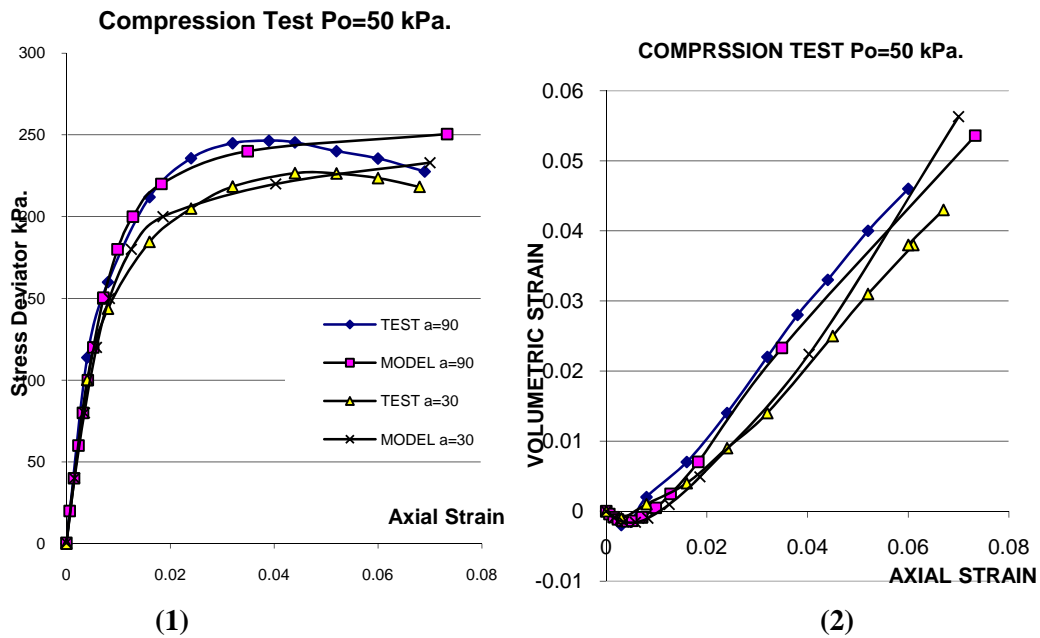


**Figure 7-a:** The comparison of stress deviator and volumetric strain versus axial strain

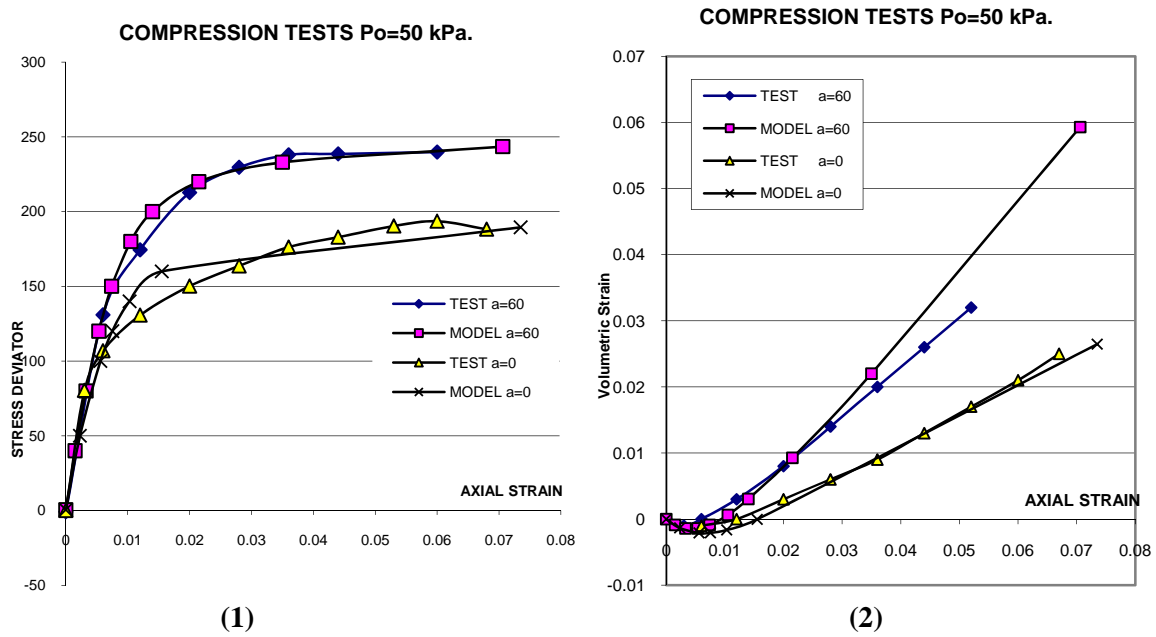


Figure 7-b: The comparison of stress deviator and volumetric strain versus axial strain

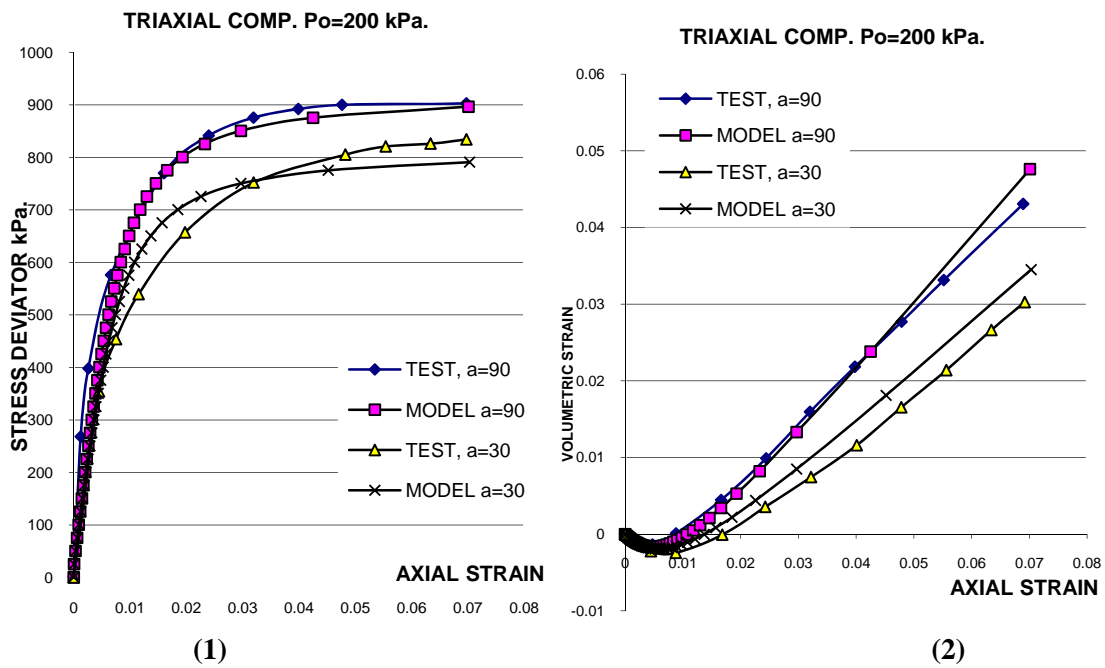


Figure 8-a: The comparison of stress deviator and volumetric strain versus axial strain

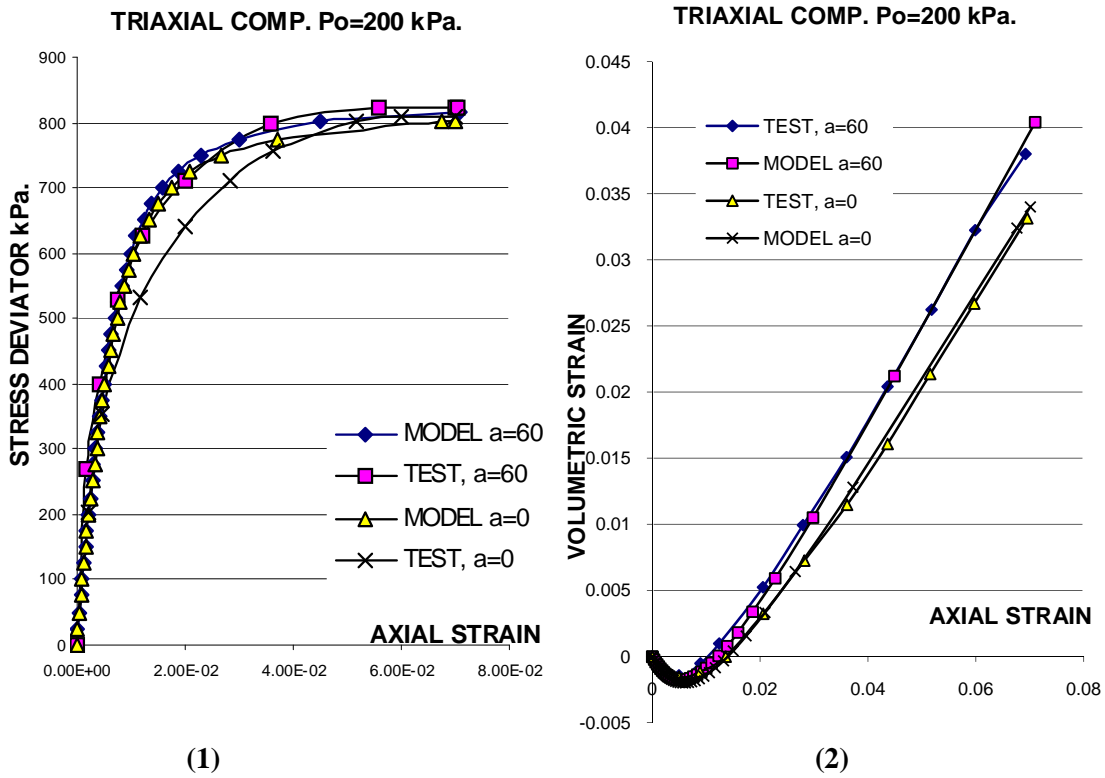


Figure 8-b: comparison of stress deviator and volumetric strain versus axial strain

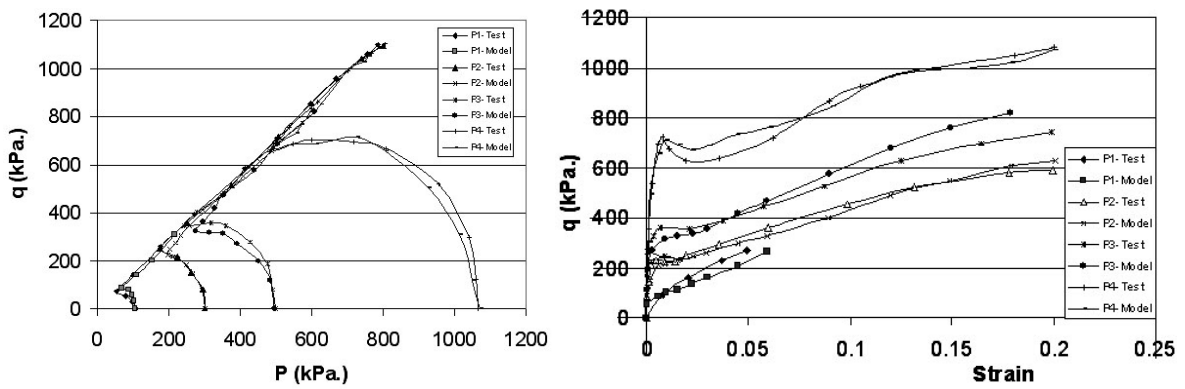


Figure 9-a: Stress paths and deviatoric stress versus axial strain in loose sand

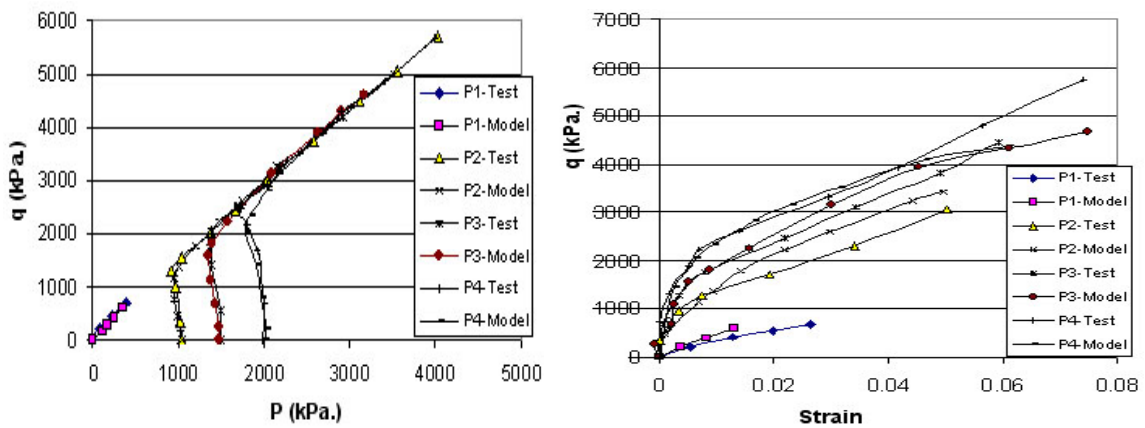


Figure 9-b: Stress paths and deviatoric stress versus axial strain in stiff sand

## CONCLUSION

A multi-plane bounding surface model is presented which simulates drained and undrained as pre- and post-liquefaction behaviour of sand. The model permits simultaneous evaluation of triggering and post-liquefaction displacement. It directly considers the reduced stiffness, strength anisotropy, and occurrence of high pore pressure ( $ru = 100\%$ ) in liquefied soils.

Triggering of liquefaction is evaluated on the nearest sampling planes orientation through liquefied elements, permitting deformation of zones of liquefaction to develop with loading in a rational manner. The effects of progressive liquefaction leading to failure, including base isolation and load shedding, are directly considered.

A micro-plane numerical algorithm is also presented for a better anticipation of load inclination effects through material. In this way, the directional information and effects of applied load orientation on mechanical behavior of material are addressed and considered. Further than possibility of predicting inherent anisotropy, this rational way facilitates to the model to predict induced anisotropy and a potential to solve anisotropy of material through defining different mechanical behavior on different orientation. This is achieved by the use of a generally simplified, applicable, effective, and easily understandable relations between micro and macro scales. These relations demonstrate an easy way to handle any heterogeneous material property as well as mechanical behavior of materials.

This model is able to solve a three dimensions plasticity problem by a rather simple theory based on the phenomenological description of plastic deformation and kinematics hardening of materials. This, is actually, achieved in such a way that the application of some difficult tasks such as induced and inherent anisotropy and rotation of principal stress and strain axes where there may be not co-axiality of them during plastic flow, to be predictable. Accordingly, the sampling plane constitutive formulations provide convenient means to classify loading events generate history rules and formulate independent evolution rules for local variables.

## REFERENCES

1. Crouch R. S. and Wolf J. P. (1994) "Unified 3D Critical State Bounding Surface Plasticity Model for Soils Incorporating Continuous Plastic Loading under Cyclic Paths. Part I: Constitutive relations," *International Journal of Numerical and Analytical Methods in Geomechanics*, 18, 735-758.
2. Dafalias Y. F. and Herrmann L. R. (1986) "Bounding surface plasticity. II: Application to isotropic cohesive soils," *Journal of Engineering Mechanics*, 112 (12) 1263-1291.
3. Been, K. and Jefferies, M. G. (1985). "A state parameter for sands." *Géotechnique*, 35(2), 99-112.
4. Zienkiewicz O.C and Pande G.N. (1977) "Time dependent multi-plane model of rocks," A numerical study of deformation and failure of rock masses, *International Journal of Numerical and Analytical Methods in Geomechanics*, 1, 219-247.
5. Sadrnejad S. A. and Pande G. N. (1989) "A multi-plane model for sands," proceeding of 3rd International Symposium of Numerical Models in Geomechanics, Niagara Falls, Canada.
6. Sadrnejad S. A. (1992) "Multi-plane elastoplastic model for granular media," *Journal of Engineering*, Islamic Republic of Iran, 5, Nos. 1&2.

7. Bazant Z. P. and Oh B. H. (1983) "Micro plane model for fracture analysis of concrete structures," Proceeding Symposium on the interaction of Non-nuclear munitions with structures, published by McGregor & Werner, Washington.
8. Hashiguchi K. and Chen Z.P. (1998) "Elastoplastic constitutive equation of soils with the subloading surface and the rotational hardening," *International Journal of Numerical and Analytical Methods in Geomechanics*, 22, 197-227.
9. Bardet J.P. (1986) "Bounding surface plasticity model for sands," *Journal of Engineering Mechanics, ASCE*, 112, 1198-1217.
10. Bardet J.P. (1990) "Hypoplastic model for sands," *Journal of Engineering Mechanics, ASCE*, 116, 1973-1994.
11. Banerjee P.K. and Yousif N.B. (1986) "A plasticity for mechanical behavior of anisotropically consolidated clay," *International Journal of Numerical and Analytical Methods in Geomechanics*, 10, 521-541.
12. Zienkiewicz O.C. and Mroz Z. (1984) "Generalized plasticity formulation and application to geomechanics," in C. S. Desai and R. H. Gallagher (eds.), *Mechanics of Engineering Materials*, Wiley, New York, 655-679.
13. Ghaboussi J. and Momen H. (1982) "Modeling and analysis of cyclic behavior of sands," G. N. Pande and O. C. Zienkiewicz (eds), *Soil Mechanics-Transient and Cyclic Loads*, Wiley, New York, 313-342.
14. Poorooshab H. B. and Pietruszczak S. (1985) "On yielding and flow of sand; a generalized two-surface model," *Computers and Geomechanics*, 1, 33-58.
15. Pietruszczak S. and Stolle D. E. F. (1987) "Modeling of sand behavior under earthquake excitation," *International Journal of Numerical and Analytical Methods in Geomechanics*, 11, 221-240.
16. Peku O. A. and Gosevski V. (1989) "Elasto-plastic model for cemented sand deposits", *Computers and Geomechanics*, 7, 155-187.
17. Somasundaram S. and Desai C. S. (1988) "modeling and testing for anisotropic behavior of soils," *Journal of Engineering Mechanics, ASCE*, 114, 1473-1496.
18. Wathugala G. W. and Desai C. S. (1993) "constitutive model for cyclic behavior of clays, I: theory," *Journal of Geotechnical engineering, ASCE*, 119, 714-729.
19. Katti D. R. and Desai C. S. (1995) "modeling and testing of cohesive soils using disturbed-state concept," *Journal of Engineering Mechanics, ASCE*, 121, 648-658.
20. Sandler I. S. and Rubin D. (1979) "An algorithm and a modular subroutine for the cap model," *International Journal of Numerical and Analytical Methods in Geomechanics*, 3, 173-186.
21. Pastor M. , Zienkiewicz O. C. and Chan A. H. C. (1990) "Generalized plasticity and the modeling of soil behavior." *International Journal of Numerical and Analytical Methods in Geomechanics*, 14, 151-190.
22. Bolzon G., Schrefler B. A. and Zienkiewicz O. C. (1996) "Elastoplastic soil constitutive laws generalized to partially saturated states," *Geotechnique*, 46, 279-289.

23. Simoni L., Salomoni V. and Schrefler B. A. (1999) "Elastoplastic subsidence models with and without capillary effects," *Computer Methods in Application Mechanics Engineering*, 171, 491–502.
24. Schrefler B. A. and Simoni L.(2000) "An elastoplastic constitutive model for partially saturated soils," In: Lemaitre J, editor. *Handbook of material behavior, nonlinear models and properties*, San Diego (CA), Academic Press.
25. Zhang H.W., Heeres O. M., de Borst R. and Schrefler B.A.(2001) "Implicit integration of a generalized plasticity constitutive model for partially saturated soil," *Engineering and Computers*, 18, 314–336.
26. Sadrnezhad, S.A. (1992) "Induced Anisotropy Prediction Through Plasticity," *Proceeding of International Conference on Engineering Applications of Mechanics*, June 9-12, Tehran, Iran, p.598-605.
27. Sadrnezhad, S.A. (1992) *Mathematical approach to Non-associated Plasticity Compliance Matrix for Granular Medium As Continuum*, *Proceeding of International Conference on "Engineering Applications of Mechanics"*, June 9-12, Tehran, Iran, p.343-349.
28. Sadrnezhad, S.A. (1998) *Prediction of The Rotation of Principal Stress Axes in Porous Media by Multi-laminate Based Model*, *Int. Journal of Univ. of Science & Tech. of Iran*, Vol. 9, No.1, pp. 15-33.
29. Sadrnezhad, S.A. (2001) "A Multi-Laminate Induced Anisotropic Double Hardening Elastoplastic Model For Sands," *Journal of Engineering, Islamic Republic of Iran*, Vol. 5, Nos.1&2, May 2001-1.
30. Sadrnezhad, S.A. (2001) "Numerical Evaluation of State Boundary Surface (Sbs) Through Rotation of Principal Stress Axes," *International Journal of Engineering, and Amir-Kabir University of Technology*, Vol. 12, No.45, WINTEWR 2001.
31. Sadrnezhad, S.A. (2002) "A Cyclic Quasi-Elastic Model for Liquefaction of Saturated Sand," *Journal of Engineering, University of Mashhad*, 11th year, no. 1.
32. Sadrnejad, S.A. (2002) "Constitutive Model for Multi-laminate Induced Anisotropic Double Hardening Elastic-Plasticity of Sand", *IJE, Transactions A: Basics*, Vol. 15, no. 2, June 2002, pp. 115-124.
33. Sadrnejad, S.A. (2006) "A General multi-plane model for Post-liquefaction of Sand," *Iranian Journal of Science & Technology, Transaction B, Engineering*, Vol. 30, No. B1, Printed in The Islamic Republic of Iran, 2006, Shiraz University

